Side-Opening Grapefruit Fiber-Based SPR Sensor for Simultaneous Measurement of Refractive Index and Temperature

Xianxing Ji, Nannan Luan, Wandi Zhang, Yaoyao Qi, Mingming Luo, and Jianfei Liu

***Abstract*—A novel side-opening grapefruit fiber-based SPR sensor is designed to realize simultaneous measurement of refractive index (RI) and temperature. The open section of the grapefruit fiber is coated with a gold layer, which can support two main resonance peaks. The variations of RI and temperature can influence the coupling efficiency between core-guided mode and plasmon mode, thus lead to the two peaks shifts that can be used to determine the variations of RI and temperature. Simulation results demonstrate that the RI coefficients of Peak I and Peak II are 1400 nm/RIU and 226 nm/RIU, respectively. The temperature coefficients of Peak I and Peak II are 34 pm/°C and 527.2 pm/°C, respectively.**

***Index Terms*—Microstructured optical fiber, optical fiber sensor, surface plasmon resonance, refractive index and temperature sensor.**

I. Introduction

SURFACE plasmon resonance (SPR) is a charge-density oscillation that may exist at the interface of the metal-dielectric surface [1]. Due to its high sensitivity to the variation of refractive index (RI), SPR sensor has attracted intensive research interest include fuel adulteration, medical diagnostic, food safety, temperature sensing, etc. [2], [3], [4], [5], [6], [7], [8]. Compared with the classical prism-based SPR sensors [9], optical fibers-based SPR sensors own the advantages include lower cost, more compact size and higher degree of integration and so on. However, in those conventional optical fiber-based sensors, the difficulty of phase matching between core-guided modes and plasmon modes is a common problem. Fortunately, this problem can be alleviated by using microstructured optical fiber (MOF), because the flexible design of MOF can tune the effective RI of Gaussian-like core mode to any desired value [10], [11], [12].

Manuscript received 13 July 2022; revised 20 October 2022; accepted 31 October 2022. Date of publication 4 November 2022; date of current version 11 November 2022. This work was supported by the Natural Science Foundation of Hebei Province under Grant F2019202294. *(Corresponding author: Nannan Luan.)*

The authors are with the Tianjin Key Laboratory of Electronic Materials and Devices, School of Electronics and Information Engineering, Hebei University of Technology, Tianjin 300401, China (e-mail: 202021902017@stu.hebut.edu.cn; nannanluan@gmail.com; 202131903016@stu.hebut.edu.cn; qiyao@hebut.edu.cn; mmluo@hebut.edu.cn; jfliu@hebut.edu.cn).

Digital Object Identifier 10.1109/JPHOT.2022.3219137

In recent years, many MOF-based SPR sensors have been proposed to detect RI [10], [11], [12], [13], temperature [14], [15], [16], pressure [17] and many other parameters [5], [18], [19]. These MOF-based SPR sensors are able to realize the detection of corresponding parameters through introducing components whose optical properties depend on each of the aiming physical parameter. However, in actual applications, it is very difficult to measure a single parameter such as RI or magnetic field due to the existence of temperature cross-sensitivity [20]. The temperature change affects the sensing performance due to the thermal expansion of the materials and the change of optical properties. To solve the impact of temperature perturbations, the most effective solution is to measure the both parameters simultaneously [21]. However, most MOF-based SPR sensors can only measure one parameter such as the RI or temperature [10], [11], [12], [13], [14], [15]. In addition, in those MOF based SPR sensors, to realize SPR sensing, the micro sized air holes are required to be coated with metal layer or filled with metal nanowires by many complicated and precise manufacture processes include pumping molten metal, wet chemistry deposition technique, and so on [10], [11], [12], [13], [14], [15]. Besides, the analytes or sensing media need to be filled into the air holes of the fiber for RI or temperature sensing, which are also very difficult procedures in actual implementation [10], [11], [12], [13], [14], [15].

More recently, the opening MOFs, including exposed-core MOFs, side-opening MOFs and side-polishing MOFs, are investigated and employed to solve the coating and filling problems in the MOF-based SPR sensors [22], [23], [24], [25], [26], [27], [28], [29], [30], [31], [32], [33], [34], [35], [36], [37], [38], [39], [40], [41]. These opening MOFs not only provide the facilitation when coating the metal layer on the opening portion, but also make the analytes being easily replaced. Moreover, the opening MOFs can also be used to simultaneously measure the RI and temperature by special designs [22], [26], [33]. In these designs, the RI detecting is implemented by coating metal layer on the opening portion and then being immersed in analyte. While the temperature sensing is realized through coating metal layer or filling nanowire into the air holes, and then filling the sensing medium into it. It should be noted that, however, the difficulties of sensor fabrication still exist when coating metal layer or placing metal wires into the air holes for temperature sensing. In this work, we design a side-opening

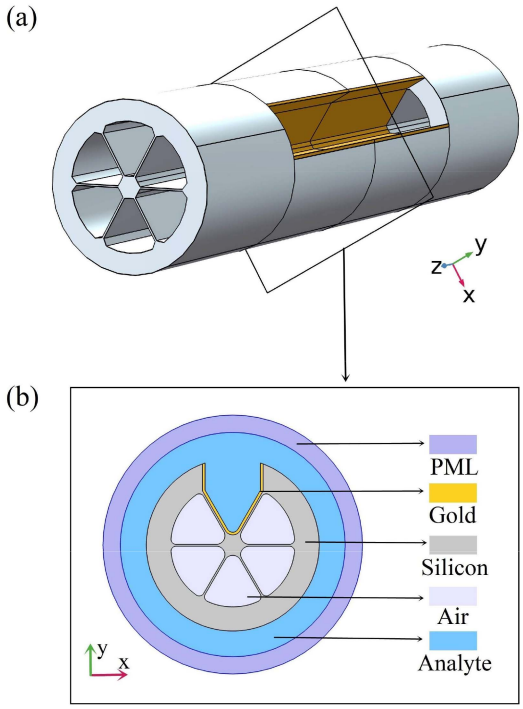

Fig. 1. (a) 3-D view of the side-opening grapefruit fiber-based SPR sensor. (b) Cross-section view of the side-opening grapefruit fiber-based SPR sensor.

grapefruit fiber based SPR sensor that not only own the capacity for simultaneous measurement of RI and temperature, but also reduce the difficulty in manufacturing process.

II. Structure and Theory

Grapefruit fibers that have six large air holes have previously been combined with SPR sensor and used for temperature sensing [15], [16]. In these previous studies, the liquid mixture that composed by ethanol and chloroform are employed as the sensing medium. In addition, the filled silver nanowires or coated silver layer can support shifty resonance peaks that corresponding to different temperature. Recently, we have demonstrated that a side-opening grapefruit based on SPR sensor can realize temperature sensing with tunable sensitivity [41]. This side-opening design is conducive to the metal coating and sensing liquid changing, which could also provide convenience for tunable sensitivity by adjust volume fraction of liquid mixture. However, this sensor can only be used to measure temperature through following one resonance peak formed by the core-guided mode coupling with the fundamental plasmon mode. In this paper, we investigate this side-opening grapefruit fiber-based SPR sensor for new sensing capacity that can measure RI and temperature simultaneously by monitoring two resonance peaks caused by the core-guided mode coupling with the fundamental and higher order plasmon modes.

Fig. 1(a) and (b) show the 3-D view and cross-section view of this grapefruit fiber based SPR sensor, respectively. As shown in Fig. 1(b), the diameters of the cladding and fiber core are 125 μm and 12 μm, respectively. The diameter of each air hole is 34.6 μm, and the center distance between adjacent air holes is 35.3 μm. In our simulation, the default RI for air is 1. For the materials of the sensor, we consider the MOF to be made by fused silica, and its RI (n_{si}) can be characterized by the dispersion equation, which is expressed as [42]:

$$n_{si}^2(\lambda,T) = (1.31552 + 0.690754 \times 10^{-5}T) + \frac{(0.788404 + 0.235835 \times 10^{-4}T)\lambda^2}{\lambda^2 - (0.0110199 + 0.584758 \times 10^{-6}T)}, + \frac{(0.91316 + 0.548368 \times 10^{-6}T)\lambda^2}{\lambda^2 - 100} \quad (1)$$

where λ is wavelength in microns and T is temperature in degrees Celsius. As for the gold material dispersion, we characterized dielectric function of gold $\varepsilon(\omega)$ by Drude-Lorentz model [10]:

$$\varepsilon(\omega) = \varepsilon_1 + i\varepsilon_2 = \varepsilon_\infty - \frac{\omega_p^2}{\omega(\omega + i\omega_c)}, \quad (2)$$

where $\omega_p = 1.3659 \times 10^{16}$ is the plasma frequency and $\omega_c = 1.45 \times 10^{14}$ is the collision frequency, and $\varepsilon_\infty = 9.75$ relates to absorption peaks in high-frequency section for gold at 298.15 K [43]. The ω_p is influenced by the variation of temperature (T) and the relationship equation between them can be described as [44]

$$\omega_p = \omega_{p0} \times \exp\left(-\frac{T - T_0}{2} \times \alpha_V(T_0)\right), \quad (3)$$

where $T_0 = 298.15$ K is the room temperature, ω_{p0} is the plasma frequency at T_0 and $\alpha_V = 4.26 \times 10^{-5}$ K^{-1} is thermal expansion coefficient for gold [29]. In addition, the collision frequency ω_{c} that contains two components include phonon-electron scattering frequency (ω_{cp}) and electron-electron scattering frequency (ω_{ce}) can be expressed as [45], [46]

$$\omega_{\mathrm{c}} = \omega_{cp} + \omega_{ce}. \quad (4)$$

The ω_{ce} is affected by temperature and it can be represented by using the Lawrence model [47]:

$$\omega_{ce}(T) = \frac{1}{6}\pi^4 \frac{\Gamma\Delta}{hE_F}\left[(k_B T)^2 + \left(\frac{h\omega}{4\pi^2}\right)^2\right], \quad (5)$$

where $\Gamma = 0.55$ is the dimensionless number [47], $\Delta = 0.77$ is fractional umklapp scattering, $h = 6.626 \times 10^{-34}$ Js is the Planck constant, $E_F = 5.51$ eV is the Boltzmann constant and $k_B = 1.38 \times 10^{-23}$ J /K is metal electrons Fermi energy [47].

The ω_{cp} is also influenced by temperature and modeled by the Holstein model [48]:

$$\omega_{cp}(T) = \omega_0\left[\frac{2}{5} + 4\left(\frac{T}{T_D}\right)^5 \int_0^{T_D/T} \frac{z^4 dz}{\mathrm{e}^z - 1}\right], \quad (6)$$

where $T_D = 170$ K is Debye temperature in degree Kelvins. The ω_0 is intraband damping coefficient [49] and it can be calculated by using the method that concluded in [14]. The value of ω_{c} is given in (2). In addition, ω_{ce} can be calculated by (5). Then the value of ω_{cp} at 298.15 K is determined by substituting the value of ω_{c} and ω_{ce} into (4). The ω_0 in (6) is able to be obtained and thus ω_{cp} at other temperature can be figured.

Equation (2)–(6) above have completely shown that the RI and temperature dependence of the dielectric constant for gold.

Besides, the Thermal Expansion of Metal Layer Is Also necessary. For Metal layer, the Linear Thermal Expansion Coefficient ($\alpha_L = \alpha_V/3$) of the bulk is not applicable here because the film may only be expanded into the normal direction [50]. Thus, a correct thermal expansion coefficient (α'_L) is required and can be expressed by a corresponding expression [50]:

$$\alpha'_L = \alpha_L \frac{1+\mu}{1-\mu}, \tag{7}$$

where $\mu = 0.44$ [50] is the Poisson number of the gold.

III. Result and Discussion

For this side-opening grapefruit MOF, it can support two fundamental core-guided modes with *x*-polarized and *y*-polarized direction [41]. The previous study has shown that the loss of this kind of side-opening grapefruit MOF at *y*-polarized resonance peak is obvious higher than that at *x*-polarized loss resonance peak. This is attribute to the fact that, compared with the *x*-polarized core-guided modes, the *y*-polarized core-guided modes are dominantly orthogonal to the surface of gold layer and couple more easily and sufficiently with the plasmon modes [23], [41], [51]. This leads to the fact that in the wavelength interrogation the *y*-polarized core-guided modes have narrower resonance peak and better signal to noise ratio. Therefore, in this work we also select the *y*-polarized core-guided modes to achieve better sensing performance in the wavelength interrogation.

Here, a finite element method (FEM) with perfect matched layer (PML) boundaries is employed to calculate the complex propagation constants of core-guided modes and plasmon modes. In theory, the couple of the two modes requires they have the approximative effective refractive (n_{eff}) [10], [11], [12], [33]. And it can be verified by observing loss spectra of the core-guided modes, which have an obvious peak at the resonance wavelength due to the energy transfers to the plasmon mode. Fig. 2(a) shows the effective refractive of *y*-polarized core-guided mode, fundamental plasmon mode and higher order plasmon mode, and the loss spectra of the *y*-polarized core-guided modes of the proposed structure with gold thickness (*m*) is 40 nm when RI (*n*) is 1.33 and temperature (*T*) is 25 °C. Fig. 2(b) shows the E field distributions of the corresponding core-guided modes and plasmon modes. In the loss spectra curve (blue solid curve) of Fig. 2(a), we can observe two main resonance peaks (Peak I and Peak II) in the wavelength range from 0.5 μm to 2 μm, which is caused by the fact that the cylindrical metal layer can support more than one type plasmon modes that can couple with the core-guided modes [10]. The insets A and B in Fig. 2(b) show the E field distributions of the core-guided mode and the fundamental plasmon mode at the wavelength of 0.5 μm and 0.56 μm. As shown, we can find that the energy of the core-guided mode and fundamental plasmon mode are mainly confined in core area and metal coated area, respectively. While their energy appears at the two areas mentioned above simultaneously at the Peak I of 0.584 μm, as shown in the inset C of Fig. 2(b), which indicate that the energy transferred from

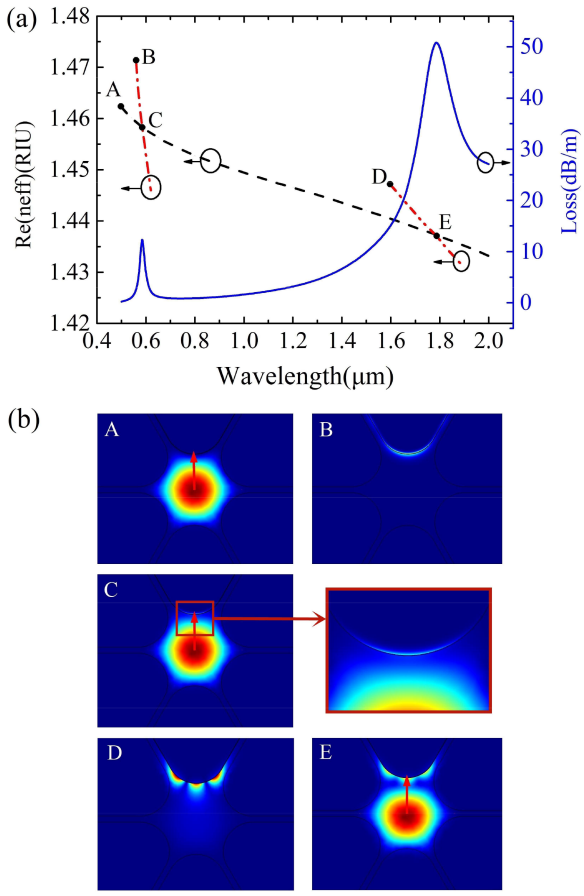

Fig. 2. (a) Dispersion relations of a core-guided mode (black dashed curve), a fundamental plasmon mode (red dashed dot curve) and a higher order plasmon mode (red dashed dot dot curve) in vicinity of the phase-matching point of the SPR sensor with m = 40 nm at $n = 1.33$ $T = 25$°C. Loss spectra of the *y*-polarized core-guided modes (blue solid curve) of the SPR sensor with m = 40 nm at $n = 1.33$ $T = 25$°C. (b) E field distributions of the corresponding modes.

core-guided mode into the plasmon mode. Similar process of energy transfer also occurs at the second resonance peak (Peak II) of 1.792 μm. However, it should be noted that the Peak II is caused by the energy transferred to higher order plasmon mode (inset D in Fig. 2(b)) from the core-guided mode as seen from the inset E of Fig. 2(b).

Fig. 3 shows the loss spectra of the *y*-polarized core-guided modes of the proposed structure at different *n* and *T* when *m* is 40 nm. The change of *n* and *T* can lead to the variation of dispersion relation of core-guided modes and plasmon modes, and then the shifts of the resonance wavelengths of the Peak I and Peak II. Here, we assume that the shift of resonance wavelength for Peak I and Peak II is $\Delta\lambda_1$ and $\Delta\lambda_2$, respectively. The influence of *n* and *T* on $\Delta\lambda_1$ and $\Delta\lambda_2$ can be given by the following relationship matrix [52]:

$$\begin{bmatrix}\Delta\lambda_1 \\ \Delta\lambda_2\end{bmatrix} = \begin{bmatrix}K_{T1} & K_{n1} \\ K_{T2} & K_{n2}\end{bmatrix} \cdot \begin{bmatrix}\Delta T \\ \Delta n\end{bmatrix} = K \cdot \begin{bmatrix}\Delta T \\ \Delta n\end{bmatrix}, \tag{8}$$

where Δn and ΔT are the variation of *n* and *T*, respectively. $K_{n1} = \Delta\lambda_1/\Delta n$ and $K_{T1} = \Delta\lambda_1/\Delta T$ represent RI and temperature coefficients for the peak I. $K_{n2} = \Delta\lambda_2/\Delta n$ and $K_{T2} =$

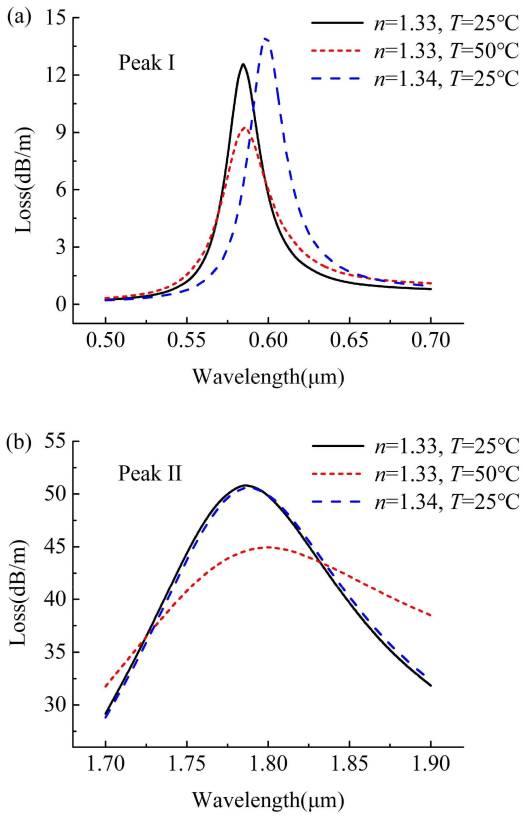

Fig. 3. Loss spectra of the *y*-polarized core-guided modes for (a) Peak I and (b) Peak II at different *n* and *T* when the *m* is 40 nm.

$\Delta\lambda_2/\Delta T$ present RI and temperature coefficients for the Peak II. According to (8), Δn and ΔT can be expressed as

$$\begin{bmatrix}\Delta T\\ \Delta n\end{bmatrix} = K^{-1}\begin{bmatrix}\Delta\lambda_1\\ \Delta\lambda_2\end{bmatrix} = \begin{bmatrix}K_{T1} & K_{n1}\\ K_{T2} & K_{n2}\end{bmatrix}^{-1}\cdot\begin{bmatrix}\Delta\lambda_1\\ \Delta\lambda_2\end{bmatrix}. \quad (9)$$

According to the data of Fig. 2, the resonance wavelengths of Peak I and Peak II all shift toward to the long wavelength with the value of RI varying from 1.33 to 1.34 at $T = 25$°C, and the RI coefficients K_{n1} and K_{n2} of them are 1400 nm/RIU and 226 nm/RIU, respectively. While the resonance wavelengths of Peak I and Peak II also shift to longer wavelengths when the temperature changes from 25°C to 50°C with $n = 1.33$, and the temperature coefficients K_{T1} and K_{T2} are 34 pm/°C and 527.2 pm/°C, respectively. It is worthy to note that the Peak I is more sensitive to the variation of the *n* while the Peak II is more sensitive to the variation of the *T*.

According to (9), the variation of *n* and *T* can be determined simultaneously by detecting the resonance wavelength shifts of Peak I and Peak II, as shown below

$$\begin{bmatrix}\Delta T\\ \Delta n\end{bmatrix} = \begin{bmatrix}-0.00030942 & 0.00191677\\ 0.00072180 & -0.00004655\end{bmatrix}\cdot\begin{bmatrix}\Delta\lambda_1\\ \Delta\lambda_2\end{bmatrix}. \quad (10)$$

Surface plasmon waves are very sensitive to the thickness of the metallic layer [10], [11], [12]. Figs. 4 and 5 display the changes in n_{eff} and loss spectra of Peak I and Peak II at $n = 1.33$ and $T = 25$°C with various *m* of 30 nm, 40 nm, and 50 nm. It can be seen from Fig. 4, as the *m* increasing, the n_{eff} curves

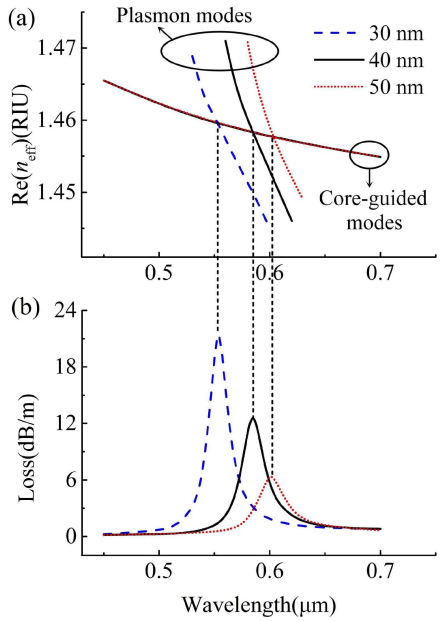

Fig. 4. (a) n_{eff} curves of the core-guided modes and the fundamental plasmon modes. (b) Loss spectra of the core-guided modes of Peak I at $n = 1.33$ and $T = 25$°C. The *m* varies for 30 nm, 40 nm and 50 nm.

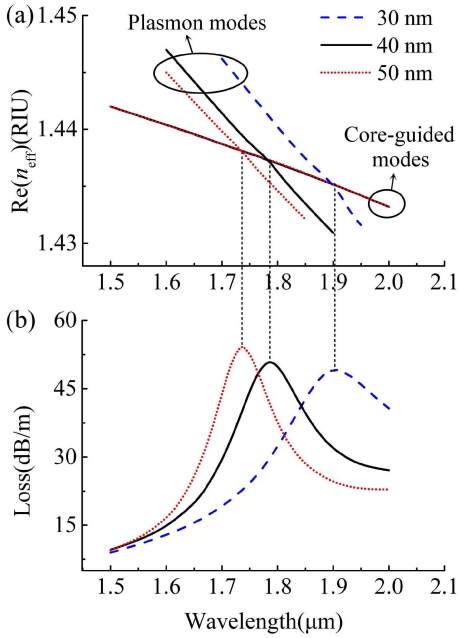

Fig. 5. (a) n_{eff} curves of the core-guided modes and the higher order plasmon modes. (b) Loss spectra of the core-guided modes of Peak II at $n = 1.33$ and $T = 25$°C. The *m* varies for 30 nm, 40 nm and 50 nm.

of plasmon modes move up, thus the intersection of n_{eff} curves of the core-guided modes and plasmon modes (phase-matching point of the peak I) shift towards to a long wavelength. However, it should be noted that the Peak II in the Fig. 5 moves to an opposite direction compared with the behavior of the peak I, because the n_{eff} of the higher order plasmon mode decreases when the *m* increases as seen from the Fig 5(a).

TABLE I
RI AND TEMPERATURE COEFFICIENTS FOR PEAK I AND PEAK II OF THE SPR SENSOR WHEN THICKNESS OF GOLD LAYER VARIERS FOR 30 NM, 40 NM AND 50 NM

m (nm)	Peak I		Peak II	
	K_n (nm/RIU)	K_T (pm/°C)	K_n (nm/RIU)	K_T (pm/°C)
30nm	1176	21.2	548	1495.2
40nm	1400	34	226	527.2
50nm	1488	48	96	339.6

To investigate the effect of m on sensitivity, we calculated RI and temperature coefficients for Peak I and Peak II when m is 30 nm, 40 nm and 50 nm in Table I. We can find that the growth of m could lead to the increase of the RI and temperature coefficients of the Peak I because of its longer resonance wavelength that promotes the plasmon penetration depth into the analyte [10]. Similarly, due to the reducing resonance wavelength of the Peak II, as m increasing, the RI and temperature coefficients decrease accordingly.

IV. CONCLUSION

We have introduced a SPR sensor that based on side-opening grapefruit fiber to measure the variation of RI and temperature simultaneously by detecting the resonance wavelength shifts of the two main peaks (Peak I and Peak II). Numerical results show that the RI coefficients of Peak I and Peak II are 1400 nm/RIU and 226 nm/RIU, respectively. The temperature coefficients of Peak I and Peak II are 34 pm/°C and 527.2 pm/°C, respectively. Moreover, the side-opening structure can also facilitate in reducing the manufacturing difficulty. Therefore, it is expected to become more competitive for detection of the two parameters in chemical and biosensing applications.

REFERENCES

[1] J. Homola, S. S. Yee, and G. Gauglitz, "Surface plasmon resonance sensors: Review," *Sens. Actuators B Chem.*, vol. 54, pp. 3–15, 1999.

[2] B. Ali, N. L. Kazanskiy, and S. N. Khonina, "Plasmonics: A necessity in the field of sensing-A review," *Fiber Integr. Opt.*, vol. 40, no. 1, pp. 14–47, Mar. 2021.

[3] K. Ahmed, M. A. Jabin, and B. K. Paul, "Surface plasmon resonance-based gold-coated biosensor for the detection of fuel adulteration," *J. Comput. Electron.*, vol. 19, no. 1, pp. 321–332, Dec. 2019.

[4] J. F. Masson, "Surface plasmon resonance clinical biosensors for medical disgnostics," *ACS Sens.*, vol. 2, no. 1, pp. 16–30, Dec. 2017.

[5] H. Thenmozhi, M. Rajan, and K. Ahmed, "D-shaped PCF sensor based on SPR for the detection of carcinogenic agents in food and cosmetics," *Optik*, vol. 180, pp. 264–270, Nov. 2019.

[6] M. S. Alam, S. Akter, B. K. Paul, and K. Ahmed, "FEM based highly sensitive dual core temperature sensor: Design and analysis," *OSA Continuum*, vol. 2, no. 9, pp. 2581–2592, Sep. 2019.

[7] B. Park et al., "Surface plasmon excitation in semitransparent inverted polymer photovoltaic devices and their applications as label-free optical sensors," *Light Sci. Appl.*, vol. 3, no. 12, Sep. 2014, Art. no. e222.

[8] J. Lao et al., "In situ plasmonic optical fiber detection of the state of charge of supercapacitors for renewable energy storage," *Light Sci. Appl.*, vol. 7, no. 1, pp. 1–11, Jul. 2018.

[9] R. Boruah, D. Mohanta, A. Choudhury, P. Nath, and A G. Ahmed, "Surface plasmon resonance-based protein bio-sensing using a Kretschmann configured double prism arrangement," *IEEE Sensors J.*, vol. 15, no. 2, pp. 6791–6796, Dec. 2015.

[10] A. Hassani and M. Skorobogatiy, "Design of the microstructured optical fiber-based surface plasmon resonance sensors with enhanced microfluidics," *Opt. Exp.*, vol. 14, no. 24, pp. 11616–11621, Dec. 2006.

[11] A. Hassani and M. Skorobogatiy, "Design criteria for microstructured-optical-fiber-based surface-plasmon-resonance sensors," *J. Opt. Soc. Amer. B*, vol. 24, no. 6, pp. 1423–1429, Jun. 2007.

[12] Y. Zhang et al., "Microstructured fiber based plasmonic index sensor with optimized accuracy and calibration relation in large dynamic range," *Opt. Commun.*, vol. 284, no. 18, pp. 4161–4166, Apr. 2011.

[13] E. Haque, S. Mahmuda, M. A. Hossain, N. H. Hai, Y. Namihira, and F. Ahmed, "Highly sensitive dual-core PCF based plasmonic refractive index sensor for low refractive index detection," *IEEE Photon. J.*, vol. 11, no. 5, Oct. 2019, Art. no. 7905309.

[14] Y. Peng, J. Hou, Z. Huang, and Q. Lu, "Temperature sensor based on surface plasmon resonance within selectively coated photonic crystal fiber," *Appl. Opt.*, vol. 51, no. 26, pp. 6361–6367, Sep. 2012.

[15] N. Luan, R. Wang, Y. Lu, and J. Yao, "Surface plasmon resonance temperature sensor based on photonic crystal fibers randomly filled with silver nanowires," *Sensors*, vol. 14, no. 9, pp. 16035–16045, Sep. 2014.

[16] N. Luan, R. Wang, Y. Lu, and J. Yao, "Simulation of surface plasmon resonance temperature sensor based on liquid mixture-filling microstructured optical fiber," *Opt. Eng.*, vol. 53, Jun. 2014, Art. no. 067103, doi: 10.1117/1.OE.53.6.067103.

[17] S. Zhang, X. Yu, P. Shum, Y. Zhang, H. P. Ho, and D. Liu, "Highly sensitive pressure-induced plasmon resonance birefringence in a silver-coated photonic crystal fiber," *J. Phys.: Conf. Ser.*, vol. 276, 2011, Art. no. 012102.

[18] S. Yao, Y. Yu, S. Qin, D. Wang, P. Yan, and Z. Zhang, "Research on optimization of magnetic field sensing characteristics of PCF sensor based on SPR," *Opt. Exp.*, vol. 30, no. 10, pp. 16405–16418, May 2022.

[19] J. N. Dash and R. Jha, "SPR biosensor based on polymer PCF coated with conducting metal oxide," *IEEE Photon. Technol. Lett.*, vol. 26, no. 6, pp. 595–598, Mar. 2014.

[20] X. Yang, Y. Lu, B. Liu, and J. Yao, "Simultaneous measurement of refractive index and temperature based on SPR in D-shaped MOF," *Appl. Opt.*, vol. 56, no. 15, pp. 4369–4374, May 2017.

[21] J. S. Velázquez-González, D. Monzón-Hernández, D. Moreno-Hernández, F. M.-P. Martínez-Pión, and I. Hernández-Romano, "Simultaneous measurement of refractive index and temperature using a SPR-based fiber optic sensor," *Sens. Actuators B: Chem.*, vol. 242, pp. 912–920, Sep. 2016.

[22] A. Chen, Z. Yu, B. Dai, and Y. Li, "Highly sensitive detection of refractive index and temperature based on liquid-filled D-shape PCF," *IEEE Photon. Technol. Lett.*, vol. 33, no. 11, pp. 529–532, Jun. 2021.

[23] N. Luan, R. Wang, W. Lv, and J. Yao, "Surface plasmon resonance sensor based on exposed-core microstructured optical fibers," *Electron. Lett.*, vol. 51, no. 9, pp. 714–715, Apr. 2015.

[24] E. Klantsataya, A. François, H. Ebendorff-Heidepriem, P. Hoffmann, and T. M. Monro, "Surface plasmon scattering in exposed core optical fiber for enhanced resolution refractive index sensing," *Sensors*, vol. 15, no. 10, pp. 25090–25102, Sep. 2015.

[25] N. Luan and J. Yao, "Surface plasmon resonance sensor based on exposed-core microstructured optical fiber placed with a silver wire," *IEEE Photon. J.*, vol. 8, no. 1, Feb. 2016, Art no. 4800508.

[26] N. Luan, C. Ding, and J. Yao, "A refractive index and temperature sensor based on surface plasmon resonance in an exposed-core microstructured optical fiber," *IEEE Photon. J.*, vol. 8, no. 2, Apr. 2016, Art. no. 4801608.

[27] N. Luan, H. Han, L. Zhao, J. Liu, and J. Yao, "Opening up dual-core microstructured optical fiber-based plasmonic sensor with1 large detection range and linear sensitivity," *Opt. Mater. Exp.*, vol. 9, no. 2, pp. 819–825, Feb. 2019.

[28] L. Zhao, H. Han, N. Luan, J. Liu, L. Song, and Y. Hu, "A temperature plasmonic sensor based on a side opening hollow fiber filled with high refractive index sensing medium," *Sensors*, vol. 19, no. 17, Aug. 2019, Art. no. 3730.

[29] J. N. Dash and R. Jha, "Highly sensitive D shaped PCF sensor based on SPR for near IR," *Opt. Quantum Electron.*, vol. 48, no. 2, pp. 1–7, Jan. 2016.

[30] J. N. Dash and R. Jha, "On the performance of graphene-based D-shaped photonic crystal fibre biosensor using surface plasmon resonance," *Plasmonics*, vol. 10, no. 5, pp. 1123–1131, Feb. 2015.

[31] N. Luan, R. Wang, W. Lv, and J. Yao, "Surface plasmon resonance sensor based on D-shaped microstructured optical fiber with hollow core," *Opt. Exp.*, vol. 23, no. 7, pp. 8576–8582, Apr. 2015.

[32] N. Luan, L. Zhao, Y. Lian, and S. Lou, "A high refractive index plasmonic sensor based on D-shaped photonic crystal fiber with laterally accessible hollow-core," *IEEE Photon. J.*, vol. 10, no. 5, Oct. 2015, Art. no. 6803707.

[33] L. Zhao, H. Han, Y. Lian, N. Luan, and J. Liu, "Theoretical analysis of all-solid D-type photonic crystal fiber based plasmonic sensor for refractive index and temperature sensing," *Opt. Fiber Technol.*, vol. 50, pp. 165–171, Jul. 2019.

[34] J. Wu, C. Dou, and L. Hu, "The D-shape elliptical stoma photonic crystal fiber based on surface plasmon resonance with both filtering and sensing," *Opt. Quantum Electron.*, vol. 53, no. 10, pp. 1–14, Sep. 2021.

[35] A. A. S. Falah, W. R. Wong, and F. R. M. Adikan, "Single-mode eccentric-core D-shaped photonic crystal fiber surface plasmon resonance sensor," *Opt. Laser Technol.*, vol. 145, Jan. 2022, Art. no. 107474.

[36] H. Han et al., "Surface plasmon resonance sensor based on dual-side polished microstructured optical fiber with dual-core," *Sensors*, vol. 20, no. 14, Jul. 2020, Art. no. 3911.

[37] H. Han et al., "A large detection-range plasmonic sensor based on an H-shaped photonic crystal fiber," *Sensors*, vol. 20, no. 4, Feb. 2020, Art. no. 1009.

[38] D. Hou et al., "Surface plasmon resonance sensor based on double-sided polished microstructured optical fiber with hollow core," *IEEE Photon. J.*, vol. 13, no. 4, Aug. 2021, Art. no. 6800408.

[39] Z. Zhang, T. Shen, H. Wu, Y. Feng, and X. Wang, "Polished photonic crystal fiber refractive index sensor based on surface plasmon resonance," *J. Opt. Soc. Amer. B*, vol. 38, no. 12, pp. F61–F68, Dec. 2021.

[40] D. Hou et al., "Surface plasmon resonance sensor based on double-sided polished microstructured optical fiber coated with graphene-on-silver layers," *IEEE Photon. J.*, vol. 14, no. 2, Aug. 2021, Art. no. 6822008.

[41] X. Ji et al., "Sensitivity-tunable temperature SPR sensor based on side-opening grapefruit fiber using liquid mixture," *IEEE Photon. J.*, vol. 14, no. 3, Jun. 2022, Art. no. 6823908.

[42] G. Ghosh, M. Endo, and T. Iwasaki, "Temperature-dependent Sellmeier coefficients and chromatic dispersions for some optical fiber glasses," *J. Lightw. Technol.*, vol. 12, no. 8, pp. 1338–1342, Aug. 1994.

[43] P. B. Johnson and R. W. Christy, "Optical constants of the noble metals," *Phys. Rev. B*, vol. 6, no. 12, pp. 4370–4379, Dec. 1972.

[44] K. Lin, Y. Lu, Z. Luo, R. Zeng, P. Wang, and H. Ming, "Numerical and experimental investigation of temperature effects on the surface plasmon resonance sensor," *Chin. Opt.*, vol. 7, no. 5, pp. 428–413, May 2009.

[45] R. T. Beach and R. W. Christy, "Electron-electron scattering in the intra-band optical conductivity of Cu, Ag, and Au," *Phys. Rev. B*, vol. 16, no. 12, pp. 5277–5284, Dec. 1977.

[46] A. K. Sharma and B. D. Gupta, "Theoretical model of a fiber optic remote sensor based on surface plasmon resonance for temperature detection," *Opt. Fiber Technol.*, vol. 12, no. 1, pp. 87–100, Aug. 2005.

[47] W. E. Lawrence, "Electron-electron scattering in the low-temperature resistivity of the noble metals," *Phys. Rev. B*, vol. 13, no. 1, pp. 5316–5319, Jun. 1976.

[48] T. Holstein, "Optical and infrared volume absorptivity of metals," *Phys. Rev.*, vol. 96, no. 2, pp. 535–536, Oct. 1954.

[49] D. F. Santos, A. Guerreiro, and J. M. Baptista, "Simultaneous plasmonic measurement of refractive index and temperature based on a D-type fiber sensor with gold wires," *IEEE Sensors J.*, vol. 17, no. 8, pp. 2439–2446, Apr. 2017.

[50] S. Herminghaus and P. Leiderer, "Surface plasmon enhanced transient thermoreflectance," *Appl. Phys. A*, vol. 51, no. 4, pp. 350–353, Oct. 1990.

[51] X. Zhang, R. Wang, F. M. Cox, B. T. Kuhlmey, and M. C. J. Large, "Selective coating of holes in microstructured optical fiber and its application to in-fiber absorptive polarizers," *Opt. Exp.*, vol. 15, no. 24, pp. 16270–16278, Nov. 2007.

[52] S. Weng, L. Pei, C. Liu, J. Wang, J. Li, and T. Ning, "Double-side polished fiber SPR sensor for simultaneous temperature and refractive index measurement," *IEEE Photon. Technol. Lett.*, vol. 28, no. 18, pp. 1916–1919, Sep. 2016.